Z^0Z^0 cross section measurement in $\ell\ell\ell'\ell'$ and $\ell\ell\nu\overline{\nu}$ final states using the full CDF dataset

CDF note 10957

The CDF Collaboration
URL http://www-cdf.fnal.gov
(Dated: January 1, 2013)

The ZZ cross section measurement is important to test Standard Model predictions of Electro-Weak couplings. Deviations from the expected values can be due to new physics that can contribute through the anomalous trilinear gauge couplings and large extra-dimensions. In addition to that, ZZ events reconstruction is important to set the scale for the $H \to ZZ$ search.
We aim to measure the ZZ production cross section through the reconstruction of the $\ell\ell\ell'\ell'$ and $\ell\ell\nu\nu$ final states. The measurements in both channels have been performed exploiting the full dataset collected by CDF experiment, corresponding to 9.7 fb^{-1} of integrated luminosity, and then combined taking into account the proper correlations. The measurement in the $\ell\ell\ell'\ell'$ decay mode is performed as a counting experiment, while in the $\ell\ell\nu\nu$ reconstruction some kinematic requirements are imposed to reduce the background contribution, and then a neural network is used to further extract the ZZ signal. The combined measured ZZ cross section is $1.38^{+0.28}_{-0.27}$ pb, in agreement with the Standard Model prediction 1.4 $\pm$ 0.1 pb at Next to Leading Order. This measurement improves the previous CDF combined ZZ production cross section measurements and is the current best measurement at the Tevatron for this process.

PACS numbers:

I. INTRODUCTION

The production of a pair of massive bosons has been largely investigated at lepton and hadron collider, and, in particular, the ZZ production cross section measurement has been an important benchmark in the validation of Standard Model (SM) predictions in the electroweak sector. This is moreover a basic step in the search of new physics, since this process is one of the dominant backgrounds for any search of exotic processes involving the production of a pair of massive bosons. The SM predicts ZZ production with a cross section of $\sigma(p\overline{p} \to ZZ)= 1.4\pm0.1$ pb at Next-to-Leading Order (NLO), which is smaller than other SM processes that can give a similar experimental signature in the detector. According to the branching ratios of a Z [1], the ZZ production can be detected in several leptonic or hadronic final states. Even if the largest decay modes involve the production of hadrons in the final state, the most interesting channels in which studying this process are the fully leptonic decay modes, given the high efficiency and precision in lepton reconstruction. The measurement described in this note focuses on the two most favorable decay channels: $\ell^+\ell^+\ell'^+\ell'^-$ and $\ell^+\ell^-\nu\overline{\nu}$.

Even if just a small amount of ZZ decays in the $\ell\ell\ell'\ell'$ final state ($\sim 0.5\%$) this process is really clean to extract a diboson signal since a negligible amount of background events can give a similar signature in the detector. No other relevant SM process gives four leptons in the final state that looks like the ones from the ZZ decay, therefore the few collected events are expected to be dominantly of the investigated signal process. The small branching fraction in this decay mode constrains the maximum precision achievable in a cross section measurement, limited by the statistics of the sample available. A parallel measurement is carried out considering the $\ell\ell\nu\nu$ decay mode which, thanks to a larger branching fraction ($\sim 3.5\%$), gives access to a larger sample of produced ZZ events. On the other hand, the presence of one $Z \to \nu\nu$ prevents from fully reconstruct the event limiting the knowledge of part of the process to global per-event properties. Several SM processes give two leptons in the final state, hence a similar signature in the detector. In particular the $Z \to \ell\ell$ production, as well as other diboson processes, lead to an overwhelming background to ZZ identification in this decay mode. The measurement in this channel has been performed exploiting an artificial neural network to extract the investigated signal process out of the background contribution in the collected data sample.

II. DETECTOR DESCRIPTION

The components of the CDF II detector relevant to this analysis are described briefly here; a more complete description can be found elsewhere [2]. The detector geometry is described by the azimuthal angle ϕ and the pseudo-rapidity $\eta \equiv -\ln(\tan\theta/2)$, where θ is the polar angle of a particle with respect to the proton beam axis (positive z-axis). The pseudo-rapidity of a particle originating from the center of the detector is referred to as $\eta_{\rm det}$.

The trajectories of charged particles are reconstructed using silicon micro-strip detectors [3, 4] and a 96-layer open-cell drift chamber (COT) [5] embedded in a 1.4 T solenoidal magnetic field. For $|\eta_{\rm det}| \leq 1$, a particle traverses all 96 layers of the COT; this decreases to zero at $|\eta_{\rm det}| \approx 2$. The silicon system provides coverage with 6 (7) layers with radii between 2.4 cm and 28 cm for $|\eta_{\rm det}| < 1.0$ ($1.0 < |\eta_{\rm det}| < 2.0$). Outside of the solenoid are electromagnetic (EM) and hadronic (HAD) sampling calorimeters segmented in a projective tower geometry. The first hadronic interaction length (λ) of the calorimeter, corresponding to 19-21 radiation lengths (X_0), uses lead absorber for measuring the electromagnetic component of showers, while the section extending to 4.5-7 λ uses iron to contain the hadronic component. The calorimeters are divided in a central ($|\eta_{\rm det}| < 1$) and forward ($1.1 < |\eta_{\rm det}| < 3.64$) region. Shower maximum detectors (SMX) embedded in the electromagnetic calorimeters at approximately $6X_0$ help in the position measurement and background suppression for electrons. Outside of the central calorimeters are scintillators and drift chambers for identifying muons as minimum ionizing particles. We use three complementary track pattern recognition algorithms which are distinguished by their starting point in COT, silicon, or projection from calorimeter energy cluster to interaction region.

III. LEPTON IDENTIFICATION

In order to maximize the signal acceptance and suppress backgrounds from jets and photons misidentified as leptons, we use ten categories of electrons and muons. Two additional categories, based on central tracks that are not fiducial to calorimeters or muon detectors, are used as either an electron or muon in forming $Z \to \ell\ell$ candidates. The resulting categories exploit essentially all the tracks and electromagnetic calorimeter clusters available.

All leptons are required to be isolated such that the sum of the E_T for the calorimeter towers in a cone of $\Delta R = \sqrt{\delta\eta^2 + \Delta\phi^2}$ <0.4 around the lepton is less than 10% of the electron E_T or muon p_T. If an additional good muon or electron candidate is found within the ΔR <0.4 cone, the towers the additional lepton passed through are subtracted

from the E_T sum. The transverse energy E_T of a shower or calorimeter tower is $E \sin\theta$, where E is the associated energy. Similarly, p_T is the component of track momentum transverse to the beam line.

Electron candidates are required to have a ratio of HAD energy to EM energy consistent with originating from an electromagnetic shower ad are further divided into central and forward categories. The central electron category require a well-measured COT track satisfying p_T >10 GeV/c that is fiducial to the central SMX and matched to a central EM energy cluster. Central electron candidates are then selected using a likelihood method to combine electron identification variables into one discriminant. A forward electron is required to be fiducial to the forward SMX detector and have energy deposition in both the calorimeter towers and SMX detector consistent with an electron shower shape. For each forward candidate, we also require a matching calorimeter seeded track that is consistent with a standalone reconstructed track formed using hits in the silicon detector to reduce background from photons. If a forward electron fails this cut based category, it has a chance to pass using likelihood based discriminant.

Muons are identified by either a charged track matched to a reconstructed track segment (*stub*) in muon chambers or as a stubless minimum ionizing particle fiducial to calorimeters. In addition, stubless muons are required to have at least 0.1 GeV in total calorimeter energy. For $\eta_{\rm det}$ <1.2, strict requirements on the number of COT hits and the χ^2 of the track fit are placed on the muon tracks in order to suppress kaon decay-in-flight backgrounds. The category of stubless muons with $|\eta_{\rm det}|$ >1.2 requires that at least 60% of the COT layers crossed by the track have hits. In order to suppress background from cosmic rays, the track's point of closest approach to the beam-line must be consistent with originating from the beam.

The final category of leptons are constructed from tracks which are not fiducial to the SMX detectors nor identified as stubbed muons. The requirements for the tracks are the same as stubless muons with $|\eta_{\rm det}|$ <1.2, but without any of the calorimeter requirements. Due to the lack of calorimeter information, electron and muons cannot be reliably differentiated in this region, and this category is therefore treated as having either flavor in the Z candidate selection. If an electron or non-fiducial track candidate is consistent with being due to a photon conversion as indicated by the presence of an additional nearby track, the candidate is vetoed.

To identify the presence of neutrinos, we define the missing transverse energy $\not\!\!E_T = |\sum_i E_{T,i} \cdot \hat{n}_{T,i}|$, where the $\hat{n}_{T,i}$ is the transverse component of the unit vector pointing from the interaction point to the calorimeter tower i. The $\not\!\!E_T$ is corrected for muons which do not deposit all of their energy in the calorimeter and tracks which point to uninstrumented regions of the calorimeter.

The ZZ candidate events are required to pass one of five online trigger selections implemented in three successively more stringent levels. The final central electron requirement is EM energy cluster with E_T >18 GeV matched to a track with p_T >8 GeV/c. Muon triggers are based on information from muon chambers matched to a track with p_T >18 GeV/c.

Selection efficiencies are measured in data and MC simulation using $Z \to \ell\ell$ samples. Correction factors are then applied to each process simulation obtained from the ratio of the efficiency calculated in the simulation and in the data.

IV. $ZZ \to \ell\ell\ell'\ell'$

A. Event selection

$ZZ \to \ell\ell\ell'\ell'$ candidate events are required to have four leptons with $p_T > 10$ GeV/c, at least one of which must have $p_T > 20$ GeV/c and be a lepton that met the trigger requirements. The leptons are grouped into opposite sign, same flavor pairs, treating the track-only leptons as either e or μ. For events containing more than one possible grouping, the grouping with the smallest sum of the differences from the Z boson mass is selected. One pair of leptons must have a reconstructed invariant mass within ± 15 GeV/c^2 of the Z mass [1], while the other must be within the range [40,140] GeV/c^2. The $ZZ \to \ell\ell\ell'\ell'$ acceptance is determined using a PYTHIA-based Monte Carlo (MC) simulation [6] including a GEANT-based simulation of the CDF II detector [7]; CTEQ5L parton distribution functions (PDFs) are used to model the momentum distribution of the initial-state partons [8].

The only significant backgrounds to the $\ell\ell\ell'\ell'$ final state come from Z+jets where two jets are misidentified as leptons and $Z\gamma$+jets where the photon and a jet are misidentified as leptons. These are estimated using a data-driven technique because the simulation is not expected to reliably model the associated rare jet fragmentation and detector effects leading to fake leptons. The probability that a jet will be misidentified as a lepton is measured using a sample of events collected with jet-based triggers and corrected for the contributions of leptons from W and Z decays. A sample of three identified leptons plus a lepton-like jet, $3l + j_l$, and two identified leptons plus two lepton-like jets, $2l + 2j_l$, is weighted with a misidentification factor to reflect the background to the $\ell\ell\ell'\ell'$ selection. This procedure double counts the contributions from Z+2 jets because these have two jets, either one of which could be misidentified to be included in the $3l + j_l$ sample, but both of which need to be misidentified to be included in the $\ell\ell\ell'\ell'$ sample. A few

percent correction is made for the double counting, and a simulation-based correction is made for the contamination of the $3l + j_l$ sample by $ZZ \to \ell\ell\ell'\ell'$ events in which one of the leptons fails the selection criteria and passes the j_l selection criteria.

The expected and observed yields are summarized in Table I, while FIG 1 shows a comparison between the MC simulation and the observed data events that pass the requirement described above.

	$\int \mathcal{L}$=9.7 fb^{-1}
Process	candidate events
ZZ	9.59 ± 1.55
$Z(\gamma)$+jets	0.06 ± 0.03
Total Expected	9.65 ± 1.55
Data	7

$ZZ \to \ell\ell\ell'\ell'$ Signal Region

TABLE I: Expected and observed number of events in the $ZZ \to \ell\ell\ell'\ell'$ signal region for the signal and background contribution.

B. Systematic uncertainties

In this cross section measurement we consider systematic uncertainties that can affect the expected signal and background contribution. We consider uncertainties of 2.5% on the acceptance due to higher order QCD effects which are not simulated, 2.7% due to PDF uncertainties, 0.04% from the trigger efficiency determination, 3.6% from the lepton reconstruction acceptance and efficiency, and 5.9% due to the luminosity uncertainty. The uncertainty on $Z(\gamma)$+jets background is determined from the variation of the jet misidentification factor among samples using different jet trigger requirements. Table II summarize the systematic uncertainties considered in the cross section measurement.

Source	ZZ	$Z(\gamma)$+jets
PDF Model	2.7 %	
Higher-order Diagrams	2.5 %	
Luminosity	5.9 %	
Jet Fake Rates		50.0 %
Lepton ID efficiencies	3.6 %	
Trigger efficiencies	0.04 %	

TABLE II: Systematic uncertainties considered in the $\ell\ell\ell'\ell'$ decay mode cross section measurement.

C. Cross section measurement

We measure the ZZ cross section using a Bayesian approach [1], building a likelihood function that express the poissonian probability to observe a number of events n for a given prediction of signal and background contribution. In the likelihood the systematic uncertainties are represented by *nuisance* parameters gaussianly constrained to zero. The likelihood function can be written as:

$$\mathcal{L}_{4\ell} = \frac{\mu^n e^{-\mu}}{n!} \cdot \prod_{j=syst.} e^{-\frac{\theta_j^2}{2}} \tag{1}$$

where n is the number of observed events, θ_j the systematic nuisance parameters, and

$$\mu = \alpha_{ZZ} \cdot \left[\prod_j (1 + f_{ZZ}^j \cdot \theta_j)\right] N_{ZZ}^{Exp} + \left[\prod_j (1 + f_{Fakes}^j \cdot \theta_j)\right] N_{Fakes}^{Exp} \tag{2}$$

where f_k^j are the fractional uncertainties for the process k corresponding to the source of systematic j, N_k^{Exp} are the nominal expected events for the signal and background processes and α_{ZZ} represent the ratio between the measured

ZZ cross section and the one used to normalize the MC. We integrate the likelihood function over the nuisance parameters θ_j (i.e. over the systematic uncertainties) obtaining the posterior probability density function (p.d.f.) $\mathcal{L}(\alpha_{ZZ})$. The value α_{ZZ} that maximizes the posterior p.d.f. is considered as the measured cross section (in units of the SM σ_{ZZ}) and the $\pm 1\sigma$ bands will define the errors on the measurement. The measured cross section in the $\ell\ell\ell'\ell'$ is

$$\frac{\sigma(p\overline{p} \to ZZ)}{\sigma_{SM}} = 0.73^{+0.31}_{-0.24}(\text{stat.})^{+0.08}_{-0.05}(\text{syst.}) = 0.73^{+0.32}_{-0.25} \ . \tag{3}$$

This result is compatible with the SM prediction and reduces the uncertainty of the previous measurement from 40% to $\sim$32%.

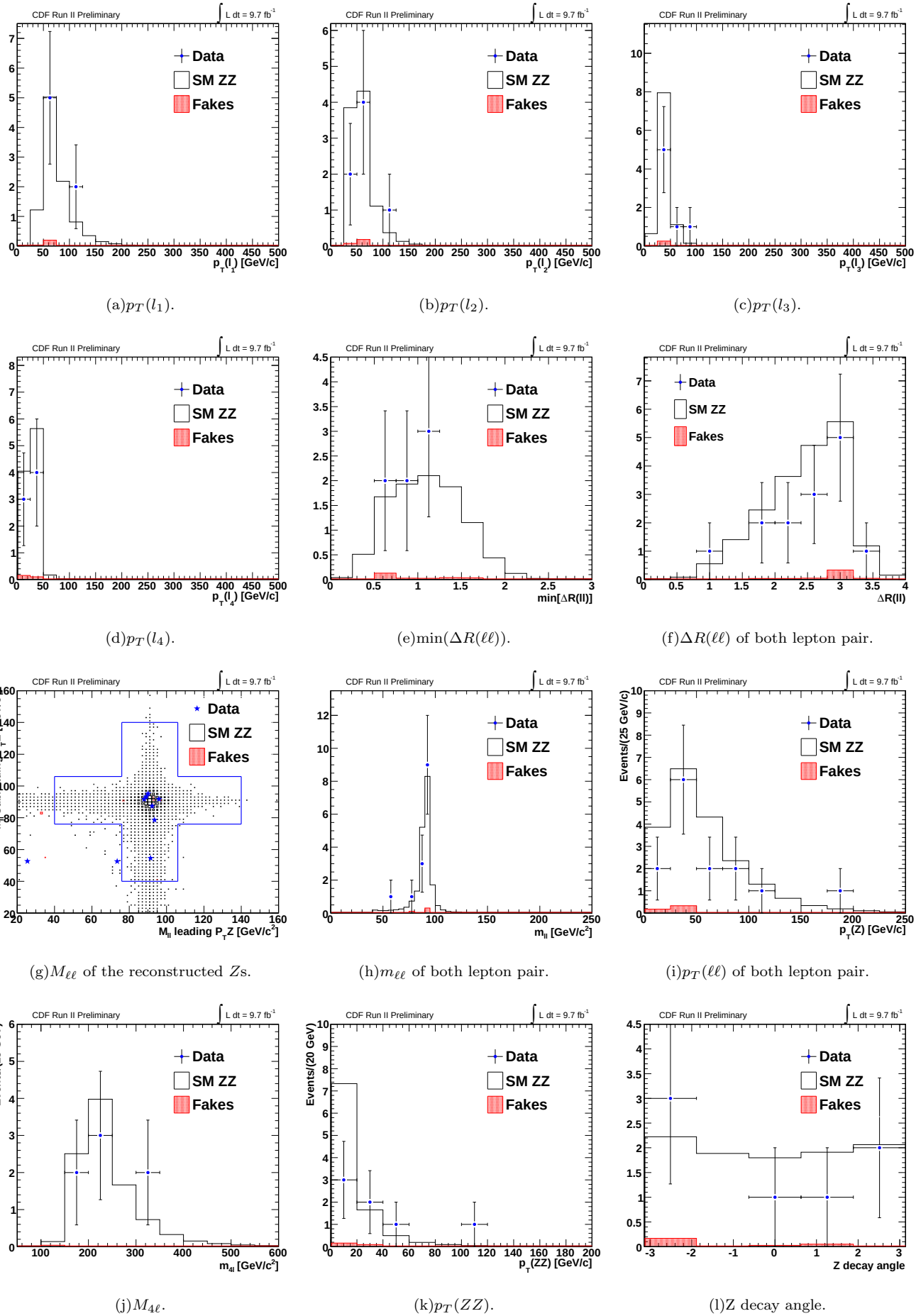

(a)$p_T(l_1)$. (b)$p_T(l_2)$. (c)$p_T(l_3)$.

(d)$p_T(l_4)$. (e)$\min(\Delta R(\ell\ell))$. (f)$\Delta R(\ell\ell)$ of both lepton pair.

(g)$M_{\ell\ell}$ of the reconstructed Zs. (h)$m_{\ell\ell}$ of both lepton pair. (i)$p_T(\ell\ell)$ of both lepton pair.

(j)$M_{4\ell}$. (k)$p_T(ZZ)$. (l)Z decay angle.

FIG. 1: Comparison of the MC simulation prediction and observation for some kinematic variables of the events in the selected $\ell\ell\ell'\ell'$ collected sample.

V. $ZZ \to \ell\ell\nu\nu$

A. Event selection

$ZZ \to \ell\ell\nu\nu$ candidates are selected among the sample of events containing exactly two leptons with the same flavor and opposite charge. One of the two leptons is required to have passed one of the considered triggers and have $p_T \geq$ 20 GeV/c, while for the second one we require $p_T \geq 10$ GeV/c. The events are selected if the two reconstructed leptons have an invariant mass within 15 GeV/c^2 of the nominal Z mass [1].

The dominant source of dilepton events is the Drell-Yan process (DY), which has a cross section many orders of magnitude larger than that of the investigated ZZ signal. The main difference between the signal and the Drell-Yan process is the presence of the two neutrinos in the signal final state which may lead to a transverse energy imbalance in the detector, quantified by the $\not\!\!E_T$. Other background contributions come from WW and WZ production, decaying in their respective leptonic channels, $W\gamma$ or W+jets production where photons or jets are misidentified as leptons, and a small contribution from $t\bar{t}$ production.

B. Data modeling

The expectation and modeling of signal and background processes are determined using different Monte Carlo (MC) simulations (as it has been done for the $\ell\ell\ell'\ell'$ final state) including a GEANT-based simulation of the CDF II detector [7]; CTEQ5L parton distribution functions (PDFs) are used to model the momentum distribution of the initial-state partons [8]. The WZ, ZZ, DY, and $t\bar{t}$ processes are simulated using PYTHIA [6] while WW is simulated using MC@NLO [9]. $W\gamma$ is simulated with the Baur event generator [10]. Each simulated sample is normalized to the theoretical cross section calculated at next-to-leading order in QCD using [11]. The W+jets background is estimated using the same data-driven technique used to evaluate the $Z(\gamma)$+jets background to the $\ell\ell\ell'\ell'$ sample. The fake lepton probabilities are applied to the jets in a W+jets enriched event sample to estimate the W+jets background contribution to our dilepton sample [12].

C. Signal Region definition

In order to extract the $ZZ \to \ell\ell\nu\nu$ signal from the background dominated sample we exploit some kinematic properties of the reconstructed event. At first, since we don't expect $\ell\ell\nu\nu$ events to have a large hadronic activity, we apply a veto on the presence of a Z-recoiling jet, rejecting events that have any jet with $E_T \geq$15 GeV and $\Delta\phi(j, Z) \geq \pi/2$. In dominant Drell-Yan background events (as well as W+jets events) is often present a high-E_T jet recoiling against the $Z \to \ell\ell$, hence this veto reduces this contribution while doesn't affect significantly the ZZ signal. This veto selects a sample composed for its ∼98% by events with no reconstructed jet at all, still dominated by Drell-Yan events.

We further select $ZZ \to \ell\ell\nu\nu$ events by requiring that the $\not\!\!E_T$ in the event is mostly aligned along the axis (Ax) of the reconstructed $Z \to \ell\ell$ in the opposite direction, selecting events with

$$\not\!\!E_T{}^{Ax} \equiv -\not\!\!E_T \cdot \cos\Delta\phi(\hat{\not\!\!E}_T, \hat{p}_T^Z) \ \geq 30 \text{ GeV}, \tag{4}$$

where $\Delta\phi(\hat{\not\!\!E}_T, \hat{p}_T^Z)$ is the angle between $\vec{\not\!\!E}_T$ and the direction of the reconstructed Z, as shown in FIG. 2. This requirement rejects 99.8% of the Drell-Yan background while preserving about 30% of the signal.

In summary, we search for the $ZZ \to \ell\ell\nu\nu$ signal in a sample of events passing the following kinematic requirements, that define the Signal Region:

- Exactly two leptons of the combination $e^+e^-e^+e^-$, $\mu^+\mu^-\mu^+\mu^-$, $e^+e^-\mu^+\mu^-$
- $p_T(\ell_1) >$20 GeV/c, $p_T(\ell_2) >$10 GeV/c
- $76 \leq M_{\ell\ell} \leq$106 GeV/c^2
- No jet with $E_T \geq$15 GeV and $\Delta\phi(j, Z) \geq \pi/2$
- $\not\!\!E_T{}^{Ax} \geq$30 GeV

The composition of the sample of events passing these requirements is summarized in TABLE III, including expectations for other minor backgrounds. FIG. 3 shows some kinematic variable comparison between data and MC simulation for events passing the Signal Region requirements.

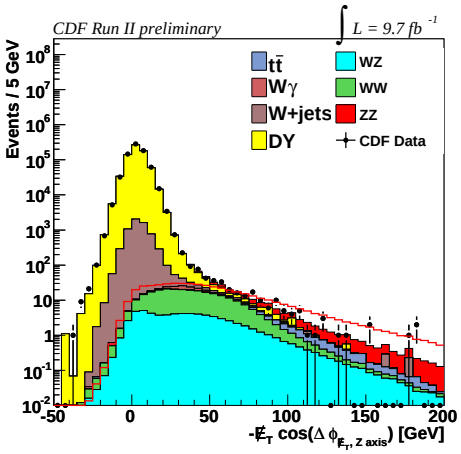

FIG. 2: $\not\!\!E_T{}^{Ax}$ distribution for the selected events (before applying the $\not\!\!E_T{}^{Ax}$ requirement, comparing data to simulation. The red line over impressed represents the ZZ signal shape, magnified $\times 5$ with respect to the proper normalization, while all the solid process contribution are stacked.

	$\int \mathcal{L} =$ 9.7 fb^{-1}
Process	candidate events
DY	317 ± 51.3
$t\bar{t}$	11.9 ± 2.2
W+jets	69.5 ± 18.5
$W\gamma$	17.3 ± 2.2
WW	114 ± 10.6
WZ	37.5 ± 5.3
Total Background	567 ± 24.4
ZZ	63 ± 11
Data	618

$ZZ \to \ell\ell\nu\nu$ Signal Region

TABLE III: Expected and observed number of events passing the kinematic requirements defining the Signal Region.

1. *Background modeling test*

The modeling of the main background contribution in the defined Signal Region (Drell-Yan, WW) have been tested in orthogonal sample of collected data with similar kinematic properties to the Signal Region. We test the Drell-Yan background modeling comparing data and simulation in a sample of events passing all the requirements applied for the Signal Region definition but having $\not\!\!E_T{}^{Ax}$ $\leq$25 GeV, where the ZZ signal contribution is negligible. The WW production modeling is tested comparing data to simulation in a sample of $e^{\pm}\mu^{\mp}$ events passing the same requirements applied for the Signal Region but $40 \leq M_{e\mu} \leq 140$ GeV/c^2, which has a negligible ZZ contribution and a small residual Drell-Yan contamination due to $Z \to \tau\tau$ decays. The discrepancies between data and Monte Carlo simulation that affects in particular the Drell-Yan modeling will be taken into account as a systematic uncertainties.

D. Neural Network separation

In order to improve the signal-to-background ratio further, we use an artificial neural network relying on the simulated samples of signal and background events. This self-learning machine exploits kinematic information about a given process (input variables) to produce an output value close to a target value (usually +1 for signal-like and -1 for background-like events). A NeuroBayes© neural network (NN) [13] is trained using seven event kinematic variables: the leading lepton transverse momentum ($p_T(\ell_1)$), the $\not\!\!E_T$ significance ($\not\!\!E_T/\sqrt{\sum E_T}$ [20]), the dilepton invariant mass ($M_{\ell\ell}$), the dilepton system transverse momentum ($p_T^{\ell\ell}$), the opening angles between the two leptons in the transverse plane ($\Delta\phi(\ell\ell)$), the number of reconstructed jets in the events (N_{jets}), and the angle in the detector transverse plane between the $\not\!\!E_T$ evaluated as the unbalance in the calorimeter towers and the $\not\!\!P_T$ representing the missing transverse p_T from the tracks reconstructed in the tracking system. These variables are the most sensitive for signal-to-background separation since they exploit the unique features of ZZ production and are shown in Figure 3, comparing data to simulations. Figure 4 shows the resulting NN output distributions for data and expected signal and background events in the Signal Region, in which ZZ signal events tend toward higher values and background toward lower values.

Exploiting the good separation of the signal from the background, we measure the ZZ cross section from a binned maximum likelihood fit of the NN output distribution. The likelihood function in the fit is the product of the Poisson

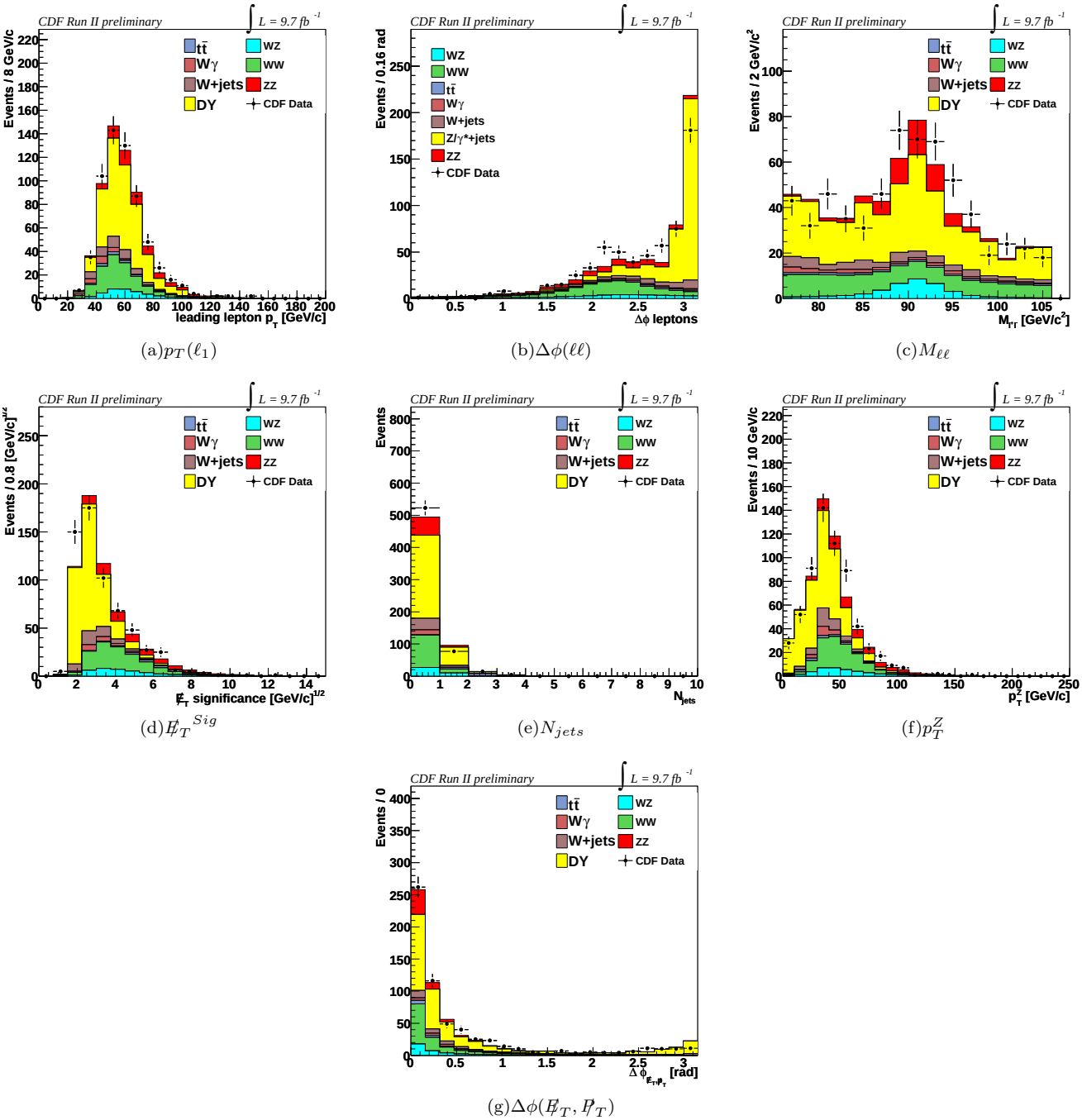

(a)$p_T(\ell_1)$ (b)$\Delta\phi(\ell\ell)$ (c)$M_{\ell\ell}$

(d)$\not\!\!E_T{}^{Sig}$ (e)N_{jets} (f)p_T^Z

(g)$\Delta\phi(\not\!\!E_T, \not\!\!P_T)$

FIG. 3: Comparison of the MC simulation prediction and observation for the kinematic variable considered in this analysis, for events passing the Signal Region requirements.

probability of the observed yield in each bin on the NN output, given the signal and background expectations.

E. Systematic uncertainties

The systematic uncertainties taken into account in this measurement can affect the shape and the normalization of the expectations of the signal and background processes contributing to the $\ell\ell\nu\nu$ final state. The shape of the Monte Carlo distributions is verified using collected data in different kinematic region and the discrepancy with respect to

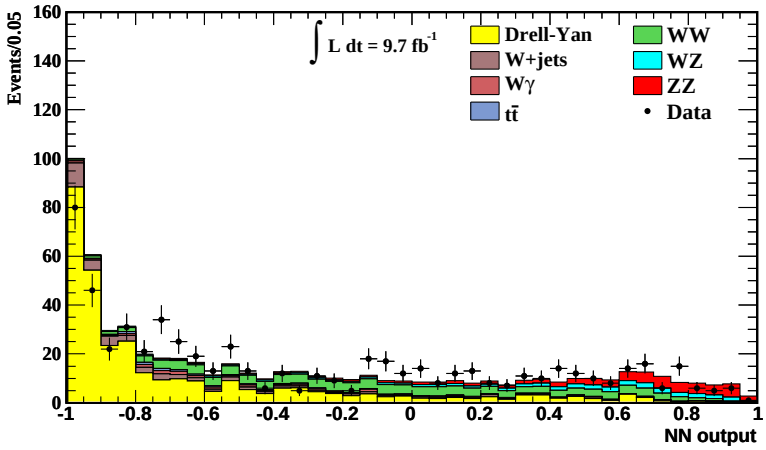

(a)

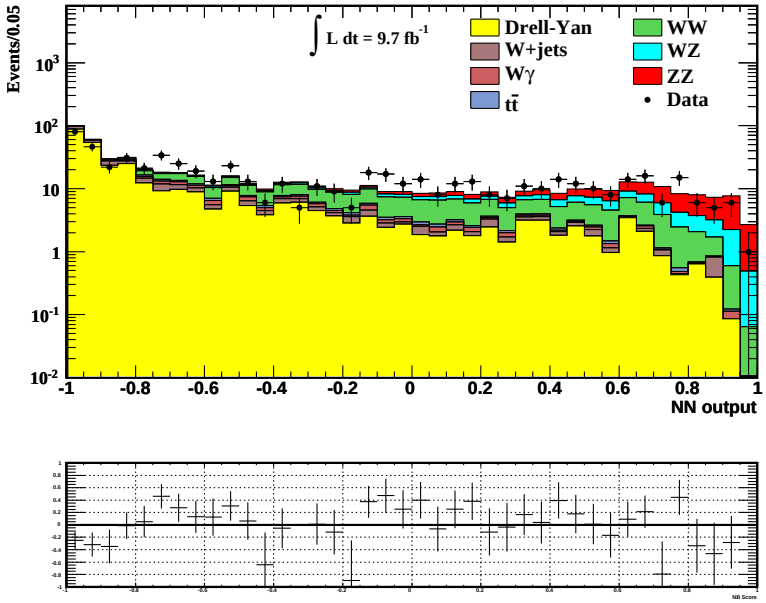

(b)

FIG. 4: Neural network output distribution for signal (in red), background expectations, with the data (dots)superimposed in (a)linear and (b)logarithmic scale.

the Monte Carlo simulation is taken into account in the cross section measurement. We also consider sources of systematic errors that can affect the theoretical prediction normalization as well as the analysis acceptance that are included in the likelihood with a Gaussian constraint to 0, and treated as nuisance parameters.

Uncertainties from measurements of the lepton selection and trigger efficiencies are propagated through the analysis acceptance. The dominant uncertainty in the final measurement comes from the acceptance difference between the leading order (LO) and the next-to-leading order (NLO) process simulation. The uncertainty in the detector acceptance is assessed using the 20 pairs of PDF sets described in [14]. We assign a 5.9% luminosity uncertainty to the normalization of MC simulated processes [15]. We include uncertainties on the theoretical cross section of WW [16], WZ [16], $W\gamma$ [17] and $t\bar{t}$ [18, 19]. The uncertainty on W+jets background is determined from the variation of the jet misidentification factor among samples using different jet trigger requirements. The effect of the uncertainty on the jet reconstructed energy is taken into account in the applied veto on the jet with $E_T > 15$ GeV/c and $\Delta\phi(j, Z) \geq \pi/2$, and in the data-to-MC reconstruction efficiency correction as function of the jet E_T. The kinematic variable distribution

mismodeling in the simulation is taken into account comparing the neural network output distribution of data and simulation, for events in the Drell-Yan and WW control region described in Section V C 1. Such neural network output distribution are shown in FIG. 5 for (a) the Drell-Yan dominated control sample and (b) the WW dominated control sample. The systematic discrepancy between data and MC simulation observed in the Drell-Yan dominated control sample is extrapolated as a systematic uncertainty affecting the shape of the NN output distribution for the Drell-Yan background prediction in the Signal Region. No significant discrepancy is observed for events in the WW dominated control sample, hence no additional systematic error is considered for the modeling of such process in the Signal Region.

All the systematic uncertainties are summarized in Table IV. Correlations between the systematic uncertainties are taken into account in the cross section measurement.

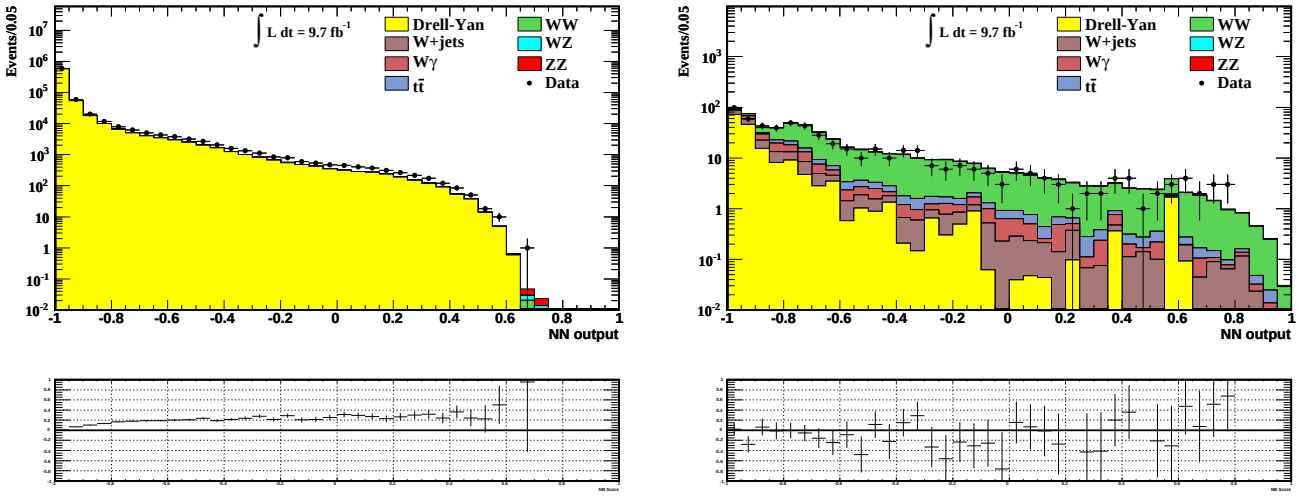

(a)Drell-Yan CR (b)WW CR

FIG. 5: Neural Network output distribution for data and simulated events in the (a) Drell-Yan Control Region and (b) WW Control Region.

Uncertainty Source	ZZ	WW	WZ	$t\bar{t}$	DY	Wγ	W+jets
Cross Section		6%	6%	10%	5%	10%	
MC-run dep.				10%			
PDF	2.7%	1.9%	2.7%	2.1%	4.1%	2.2%	
NLO	5%		5%	10%		5%	
$\mathcal{L}$	5.9%	5.9%	5.9%	5.9%	5.9%	5.9%	
Conversion						10%	
Jet Modeling	2.0%	1.6%	3.4%	5.3%	6.2%	2.0%	
Fakes							16%
Lepton ID Eff.	3%	3%	3%	3%	3%		
Trigger Eff.	2%	2%	2%	2%			
NN shape					*shape*		

TABLE IV: Systematic uncertainties considered in the cross section measurement in the $\ell\ell\nu\nu$ decay mode.

F. Cross section measurement

The ZZ production cross section is measured from the binned Neural Network output distribution, considering all the systematic uncertainties that might affect the normalization of the MC predictions as well as the shape of the NN output distributions described before. The same Bayesian approach used for the cross section measurement in the

$\ell\ell\ell'\ell'$ decay channel is applied in this case defining a likelihood function

$$\mathcal{L}_{\ell\ell\nu\nu} = \left(\prod_i \frac{\mu_i^{n_i} e^{-\mu_i}}{n_i!} \right) \cdot \prod_{j=syst.} e^{-\frac{\theta_j^2}{2}} \tag{5}$$

where the index i runs over the bins of the NN output distribution, n_i is the number of events observed in the i-th bin of the distribution, the *nuisance* parameters θ_j represent the systematic uncertainties and are gaussianly constrained to 0, and

$$\mu_i = \sum_k \alpha_k \left[\prod_j (1 + f_k^j \cdot \theta_j) \right] (N_k^{Exp})_i \tag{6}$$

where f_k^j are the fractional uncertainties for the process k corresponding to the systematic j, and N_k^{Exp} are the expected number of events for the several processes in each bin. The parameters α_k are all fixed to 1 (i.e. the predictions are fixed to the nominal MC normalization) but α_{ZZ}.

We extract the cross section (in units of the SM prediction σ_{SM}^{ZZ}) from the $\mathcal{L}_{\ell\ell\nu\nu}(\alpha_{ZZ})$ posterior p.d.f. obtained after integrating over all the nuisance parameters:

$$\frac{\sigma(p\overline{p} \to ZZ)}{\sigma_{SM}} = 1.06^{+0.24}_{-0.22}(\text{stat.}) \pm 0.12(\text{syst.}) = 1.06^{+0.27}_{-0.25} \ . \tag{7}$$

The result is in really good agreement with the SM prediction, reducing the uncertainty on the central value to ∼27%, with respect to the 45% uncertainty of the previous CDF measurement in this decay channel.

VI. COMBINED RESULT

After measuring separately the ZZ production cross section in the $\ell\ell\ell'\ell'$ and $\ell\ell\nu\overline{\nu}$ we can combine these two result, taking into account the proper correlations between the measurements in the two separate decay modes. In this case the posterior p.d.f. is obtained from the product of the probabilities in the two decay channel, with a common term representing the systematic uncertainties gaussianly constrained. The combined likelihood is then:

$$\mathcal{L} = \mathcal{L}_{\ell\ell\nu\nu} \otimes \mathcal{L}_{4\ell} = \left[\left(\prod_i \frac{\mu_i^{n_i} e^{-\mu_i}}{n_i!} \right)_{NN} \times \frac{\mu_{4\ell}^{n_{4\ell}} e^{-\mu_{4\ell}}}{n_{4\ell}!} \right] \cdot \prod_{j=syst.} e^{-\frac{\theta_j^2}{2}} \ . \tag{8}$$

The core of the likelihood is composed by the product of the probabilities in each bin of the Neural Network output and the one corresponding to the four lepton analysis. With such definition of the likelihood function are automatically correlated all the systematic uncertainties parameters shared by the two decay modes. The posterior p.d.f., $\mathcal{L}(\alpha_{ZZ})$, gives as a result

$$\frac{\sigma(p\overline{p} \to ZZ)}{\sigma_{SM}} = 0.99 \pm 0.14(\text{stat.})^{+0.14}_{-0.13}(\text{syst.}) = 0.99^{+0.20}_{-0.19} \ . \tag{9}$$

This corresponds to a measured ZZ production cross section in the zero-width approximation[21] of

$$\sigma(p\overline{p} \to ZZ) = 1.38 \pm 0.19(\text{stat.})^{+0.20}_{-0.19}(\text{syst.}) = 1.38^{+0.28}_{-0.27} \text{ pb} \tag{10}$$

which is in really good agreement with the Standard Model prediction, σ_{ZZ}^{NLO}= 1.4±0.1 pb, and significantly improves the previous CDF combined measurement, reducing the uncertainty from ∼28% to ∼20%.

[1] K. Nakamura et al. (Particle Data Group), J.Phys. G **37**, 075021 (2010).
[2] R. Blair, *et al.* (CDF Collaboration) (1996), FERMILAB-PUB-96/390-E.
[3] A. Sill *et al.*, Nucl. Instrum. Methods A **447**, 1 (2000).
[4] A. Affolder *et al.*, Nucl. Instrum. Methods A **453**, 84 (2000).
[5] T. Affolder *et al.*, Nucl. Instrum. Methods A **526**, 249 (2004).

[6] T. Sjostrand, S. Mrenna, and P. Skands, JHEP **05**, 026 (2006).
[7] R. Brun *et al.*, version 3.15, CERN-DD-78-2-REV.
[8] H. L. Lai *et al.* (CTEQ), Eur. Phys. J. **C12**, 375 (2000).
[9] S. Frixione and B. R. Webber, JHEP **06** (2002), hep-ph/0204244.
[10] U. Baur and E. L. Berger, Phys. Rev. **D47**, 4889 (1993).
[11] J. Campbell and R. K. Ellis, *MCFM - Monte Carlo for FeMtobarn processes* (2010), We ran MCFM Monte Carlo with the MSTW2008 PDF set and varying the factorizzation and renormalizzation scale.
[12] S.-C. Hsu, Ph.D. thesis, UC, San Diego (2008), FERMILAB-THESIS-2008-61.
[13] M. Feindtz and U. Kerzel, Nucl. Instr. Meth. **A**, 190 (2006).
[14] S. Kretzer, H. L. Lai, F. I. Olness, and W. K. Tung, Phys. Rev. **D69**, 114005 (2004).
[15] D. Acosta *et al.*, Nucl. Instrum. Meth. **A494**, 57 (2002).
[16] J. Campbell and R. K. Ellis, Phys. Rev. D **60**, 113006 (1999).
[17] U. Baur, T. Han, and J. Ohnemus, Phys. Rev. D **57**, 2823 (1998).
[18] N. Kidonakis and R. Vogt, Phys. Rev. **D68**, 114014 (2003).
[19] M. Cacciari, S. Frixione, M. L. Mangano, P. Nason, and G. Ridolfi, JHEP **04**, 068 (2004).
[20] $\sum E_T$ is defined as the sum of the energy deposit in the calorimeter towers times the sine of the polar angle of the tower.
[21] The zero-width approximation for the cross section calculation is the proper value to quote since it is independent from the considered ZZ decay mode, hence easy to compare with other cross section measurements.